PRAMANA — journal of physics

Vol. 79, No. 1
July 2012
pp. 95–106

Effect of hydrostatic pressure on the structural, elastic and electronic properties of (B3) boron phosphide

SALAH DAOUD[1,*], KAMEL LOUCIF[2], NADHIRA BIOUD[3], NOUDJOUD LEBGAA[3] and LAARBI BELAGRAA[4]

[1]Institut des Sciences et Technologies, Centre Universitaire de Bordj Bou Arreridj, Bordj-Bou-Arreridj, Algérie
[2]Laboratoire Des Matériaux Non Métalliques, Université Ferhat Abbes-Sétif, Sétif, Algérie
[3]Laboratoire d'Optoélectronique & Composants, Université Ferhat Abbes-Sétif, Sétif, Algérie
[4]Laboratoire Matériaux et Systèmes Electroniques, Centre Universitaire de Bordj Bou Arreridj, Bordj-Bou-Arreridj, Algérie
*Corresponding author. E-mail: salah_daoud07@yahoo.fr

MS received 31 December 2011; accepted 23 January 2012

Abstract. In this paper we present the results obtained from first-principles calculations of the effect of hydrostatic pressure on the structural, elastic and electronic properties of (B3) boron phosphide, using the pseudopotential plane-wave method (PP-PW) based on density functional theory within the Teter and Pade exchange-correlation functional form of the local density approximation (LDA). The lattice parameter, molecular and crystal densities, near-neighbour distances, independent elastic constants, bulk modulus, shear modulus, anisotropy factor and energy bandgaps of (B3) BP under high pressure are presented. The results showed a phase transition pressure from the zinc blende to rock-salt phase at around 1.56 Mbar, which is in good agreement with the theoretical data reported in the literature.

Keywords. Hydrostatic pressure effect; structural, elastic and electronic properties; (B3) boron phosphide.

PACS Nos 45.10.Ab; 62.20.Dx; 81.05.Ea; 31.15.E-

1. Introduction

Many III–V semiconductor compounds, crystallize in the cubic zinc-blende structure, which closely resembles diamond structure in these compounds, where the atoms are tetrahedrally bonded to four nearest neighbours through covalent bonds [1,2]. Under hydrostatic pressure, the low-pressure phase is destabilized and structural phase transition occurs. For boron phosphide (BP), the phase transition pressure occurs at 150 GPa [3]. Theoretical study of the pressure dependence of second-order elastic constants was carried out by Herrera-Cabrera *et al* [4]. Even though BP has interesting properties such as hardness, high melting point and resistance to corrosion [5], which make it a promising

DOI: 10.1007/s12043-012-0283-8; ***e*Publication: 9 May 2012**

material in optoelectronic devices [6], theoretical knowledge of this material is, unfortunately very limited [7–9]. The data on phonon spectra and vibrational properties are also very little [10,11]. Cardona *et al* [12,13] used Raman scattering to study the effect of pressure on the lattice dynamics of III–V compounds up to phase transition pressure, in which Raman scattering reveals phase transition as discontinuities in phonon frequencies or intensity of phonon peaks. Recently, Shinde *et al* [14] used rigid ion model (RIM) and deformation bond approximation (DBA) model to study the pressure dependence of phonon dispersion, phonon density of states, mode Grüneisen parameters and specific heat for some III–B semiconductors.

In the present work, we report first principles study of the effect of hydrostatic pressure on the structural and elastic properties, the lattice parameter, molecular and crystal densities, nearest-neighbour and near-neighbour distances, independent elastic constants C_{ij}, bulk modulus B, shear modulus G, anisotropy factor A, energy bandgaps E_i and stability criteria for boron phosphide in its zinc blende phase, using the state-of-the-art pseudopotential plane-wave method (PP-PW), in the framework of the density functional theory (DFT) within the local density approximation (LDA).

The paper is organized as follows: In §2, we briefly describe the computational techniques used in this work. Results and discussions are presented in §3. Finally, conclusions and remarks are given in §4.

2. Computational methods

The first-principles calculations were performed by employing pseudopotential plane-wave (PP-PW) approach based on the density functional theory (DFT) [15] and implemented in the ABINIT code [16].

ABINIT computer code is a common project of the Université Catholique de Louvain, Corning Incorporated, and other contributors. We used the Teter and Pade (fitting of PW92 data) parametrization [17] for LDA. Only the outermost electrons of each atom were explicitly considered in the calculation. The effect of the inner electrons and the nucleus (the frozen core) was described within a pseudopotential scheme. We used the Trouiller–Martins scheme [18] to generate the norm-conserving nonlocal pseudopotentials, which results in highly transferable and optimally smooth pseudopotentials.

A plane-wave basis set was used to solve the Kohn–Sham equations in the pseudopotential implementation of the DFT-LDA. Major advantages of this approach are: the ease of computing forces and stresses; good convergence control with respect to all employed computational parameters; favourable scaling with the number of atoms in the system and the ability to make cheaper calculations by neglecting core electrons.

The two parameters that affect the accuracy of calculations are the kinetic energy cut-off which determines the number of plane-waves in the expansion and the number of special k-points used for the Brillouin zone (BZ) integration. The BZ integrations were replaced by discrete summations over a special set of k-points, using the standard k-point technique of Monkhorst and Pack [19] where the k-point mesh used is $(2 \times 2 \times 2)$. The plane-wave energy cut-off to expand the wave functions is set to be 60 Hartree (1 Hartree = 27.211396 eV). Careful convergence tests show that with these parameters, the relative energy is converged to better than 10^{-5} eV/atom.

3. Results and discussions

3.1 *Structural properties at zero pressure*

After determining the kinetic energy cut-off and the number of special k-points which give the best possible convergence of total energy, they are used to calculate the total energy for various lattice constants. Energies were calculated for various lattice constants and the different values obtained were then traced as functions of unit cell volume. One can deduce the static structural properties such as the equilibrium lattice constant from the volume which gives the minimum energy, bulk modulus B_0 and its pressure derivatives B_0'. The procedure consisted of fitting the values of total energy as functions of the unit cell volume using the Murnaghan equation [20] given by

$$E(V) - E(V_0) = \frac{B_0 V}{B_0'}\left[\frac{(V_0/V)^{B_0'}}{B_0' - 1} + 1\right] - \frac{B_0 V_0}{B_0' - 1}, \tag{1}$$

$$B_0 = V\frac{\partial^2 E}{\partial V^2} = \frac{4}{9a}\frac{\partial^2 E}{\partial a^2}, \tag{2}$$

where B_0 is the bulk modulus given by eq. (2) at $P = 0$, V_0 is the equilibrium volume, $E(V_0)$ is the energy in equilibrium volume, B_0' is the pressure derivative of the bulk modulus at $P = 0$ and a is the lattice constant.

Figure 1 shows the evolution of total energy as a function of the unit cell volume of (B3) BP.

The equilibrium lattice parameter is computed from the structural optimization, using the Broyden–Fletcher–Goldfarb–Shanno minimization (BFGS) [21].

The results for lattice parameter a_0 obtained from the fit of the Murnaghan equation and from the BFGS technique, bulk modulus B_0, and its pressure derivative B_0' are reported in table 1 and compared with the available experimental [22–24] and theoretical data [7,8,25–27].

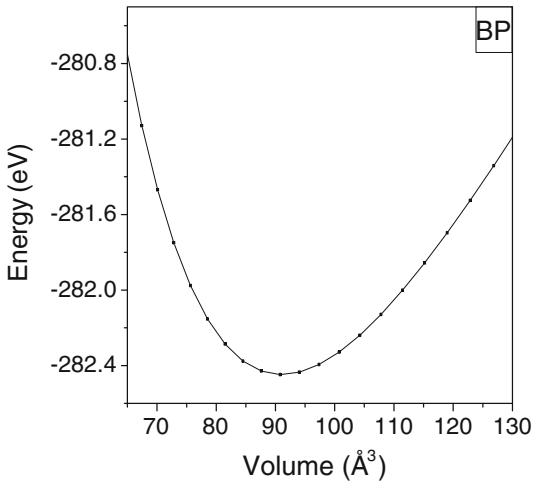

Figure 1. Evolution of the total energy as a function of the unit cell volume.

Table 1. Structural parameters of (B3) BP at zero pressure. A comparison of lattice constants a_0, bulk modulus B_0 and its pressure derivative B_0' with experimental [22–24] and theoretical [7,8,25–27] values can also be seen.

a_0 (Å)	4.494[a]	4.516[b]	4.53 [7]	4.538 [22]	4.5383 [23]	4.546 [25]	4.51 [26]	4.558 [8,27]
B_0 (Mbar)	1.667[a]		1.52 [7]	1.65 [8]	1.73 [24]	1.70 [25]	1.72 [26]	1.66 [27]
B_0'	3.743		4.3 [7]	3.07 [25]	3.7 [26]			

[a]From the Murnaghan equation (1).
[b]From the BFGS technique.

As can be seen, our calculated equilibrium lattice parameter (a_0) in the two cases is in good agreement with the experimental data and previous calculations: the BFGS-calculated lattice constant deviates from the measured [22] and the calculated [26] ones within 0.48% and 0.13% respectively. We can also see that our calculated bulk modulus B_0 obtained from eq. (2) is in good agreement with the experimental data and previous calculations, and it deviates from the measured [24] and the calculated [27] ones within 3.64% and 0.42% respectively. The pressure derivatives of the bulk modulus B_0' is also in good agreement with the available theoretical data [26]. These results show that the computational methods and parameters used in this paper are reasonable.

Many theoretical approaches [28–30] have been reported recently to determine the cohesive energy of solid-state compounds. Schlosser [31] has studied the cohesive energy trends in rock-salt structure in terms of nearest-neighbour distance. Verma *et al* [32] have studied the cohesive energy trends in zinc-blende ($A^{III}B^{V}$ and $A^{II}B^{VI}$) structured compounds in terms of nearest-neighbour distance using the following relation:

$$E_{\text{coh}} = \text{cons. tan } t\frac{(Z_1 Z_2)^{0.4}}{d^{2.5}}, \tag{3}$$

where Z_1 and Z_2 are ionic charges of the cation and anion respectively and d is the nearest-neighbour distance in Å. The value of constant for zinc blende-type crystal structure is 710. The value of the product of ionic charge is 4 for $A^{II}B^{VI}$ and 9 for $A^{III}B^{V}$ semiconductors [33]. The proposed theoretical relation (5) has been applied to evaluate (B3) BP compound. The result obtained is about 319.75 kcal/mol.

3.2 *Effect of hydrostatic pressure*

3.2.1 *Lattice constant and the relative changes of the lattice constant parameter.* To further validate the reliability and accuracy of our calculated structural properties for (B3) BP, the calculated unit cell volumes under a series of applied hydrostatic pressure were used to construct the *P–V* dataset, which was subsequently fitted by the Murnaghan equation [20].

$$P = \frac{B_0}{B_0'}\left[\left(\frac{a_0}{a(p)}\right)^{3B_0'} - 1\right], \tag{4}$$

where B_0 is the bulk modulus, B_0' is its pressure derivative at zero pressure, a_0 is the equilibrium lattice constant and $a(p)$ is the lattice constant when $P \neq 0$.

Effect of hydrostatic pressure

The equilibrium geometries of (B3) BP unit cells were computed at fixed values of applied hydrostatic pressure in the 0 to 1.5 Mbar range in steps of 0.25 Mbar, where, at each pressure, a complete optimization for the unit cell volume was performed. In figure 2, the variation of the unit cell volume vs. applied hydrostatic pressure is presented.

The continuity of the volume in pressure–volume (*PV*) phase diagram indicates the stability of the (B3) structure, and hence the absence of structural phase transition from the zinc blende (B3) to rock-salt (B1) till the pressure reaches 1.5 Mbar.

3.2.2 *Molecular and crystal densities and near-neighbour and nearest-neighbour distances.* The crystal density g, one of the simplest and most important material parameters, is related to the atomic arrangement and the corresponding electron density map. Group IIIb atoms have three electrons with an s^2p^1 configuration outside a core of closed shells, and group Vb atoms have five electrons in an s^2p^3 configuration. The IIIb and Vb atoms have, therefore, an average of four valence electrons per atom available for bonding. For such a covalent bonding, each V atom donates an electron to a III atom, so that V^+ and III^- ions are formed, each with four valence electrons. An ionic bond is due to the Coulomb attraction between the excess positive and negative charges on ions formed by the transfer of electrons from the metallic to the nonmetallic atom. The bonds in most of the III–V compounds are not adequately described by any of these extreme types, but have characteristics intermediate between those usually associated with the terms covalent and ionic.

There are four molecules in a unit cell of the zinc blende lattice. If an accurate lattice constant is available, the calculation of g gives, in principle, a good and reliable value.

For BP each B(P) has four nearest neighbours of P(B) at a distance of $\sqrt{3}a_0/4$ at the corners of a regular tetrahedron. The spacing between the near-neighbour B–B (P–P)

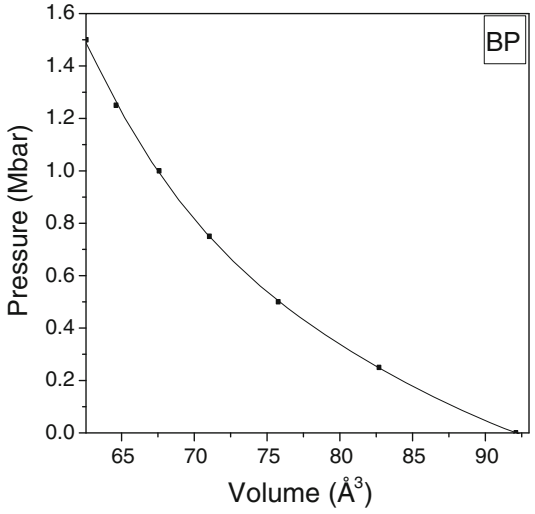

Figure 2. Pressure–volume dependence of the (B3) BP compound.

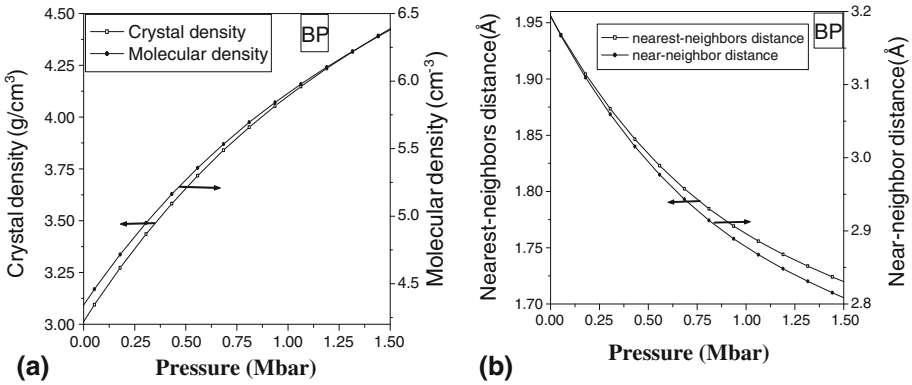

Figure 3. (**a**) Crystal and molecular densities, (**b**) nearest-neighbour and near-neighbour distances vs. the hydrostatic pressure of the (B3) BP compound.

atoms is equal to $a_0/\sqrt{2}$. The calculated molecular and crystal densities, and the near-neighbour and nearest-neighbour distances using the lattice constant obtained from the Murnaghan equation (1) for (B3) BP at zero temperature are plotted in figure 3.

3.2.3 *Elastic stiffness constants.* The number of independent elastic constants is usually reduced if the crystal possesses symmetry elements, and in the important case of cubic crystals there are only three independent stiffness constants. The array of values of the elastic stiffness constant is therefore reduced for a cubic crystal to the matrix [C] [34].

$$[\mathrm{C}] = \begin{bmatrix} C_{11} & C_{12} & C_{12} & 0 & 0 & 0 \\ C_{12} & C_{11} & C_{12} & 0 & 0 & 0 \\ C_{12} & C_{12} & C_{11} & 0 & 0 & 0 \\ 0 & 0 & 0 & C_{44} & 0 & 0 \\ 0 & 0 & 0 & 0 & C_{44} & 0 \\ 0 & 0 & 0 & 0 & 0 & C_{44} \end{bmatrix}. \tag{5}$$

In a cubic lattice, three independent elastic constants C_{11}, C_{12} and C_{44} are determined by employing suitable lattice distortions. Following the work of Nielsen and Martin [35], we determine these constants. Values for C_{11} and C_{12} can be found from the stress–strain relation by applying ε_1 strain. This strain scales the x-dimensions by $(1 + \varepsilon_1)$ while maintaining constant y- and z-dimensions. For small strain, the harmonic approximation defines the relations as

$$C_{11} = \frac{\sigma_1}{\varepsilon_1}, \tag{6}$$

$$C_{12} = \frac{\sigma_2}{\varepsilon_1}, \tag{7}$$

where σ_i $(i = 1, 2)$ represent the stress.

From the following stress–strain relation [35]

$$\sigma_4 = \left[C_{44}^0 - \Omega^{-1} \Phi \left(\frac{\xi a_0}{4} \right)^2 \right] \varepsilon_4 = C_{44} \varepsilon_4, \tag{8}$$

one can obtain the elastic constant $C_{44} = \sigma_4/\epsilon_4$. In eq. (8), C_{44}^0 denotes the elastic constant in the absence of internal displacement u, Ω is the volume of the unstrained unit cell, Φ is the force constant and ξ is the internal strain parameter. With two independent calculations, setting $\varepsilon_4 = 0$ and a small relative displacement u and then with small ε_4 and $u = 0$, we can determine C_{44} and ξ (details of this method can be found in ref. [35]). The calculation was performed with $\varepsilon_1 = \pm 0.002$ in the direction (1 0 0) to determine C_{11} and C_{12} and with $\varepsilon_4 = \pm 0.004$ and $u = \pm 0.002\sqrt{3}a_0$ in the direction (1 1 1) to find C_{44} and ξ. For cubic crystals, the bulk modulus B is related to elastic constants C_{11} and C_{12} by [34]

$$B = \left[\frac{(C_{11} + 2C_{12})}{3}\right]. \tag{9}$$

The obtained elastic constants C_{11}, C_{12}, C_{44} and the bulk modulus B of (B3) BP at different pressure are presented in figure 4.

3.2.4 *Shear modulus G and the anisotropy factor A.* The shear modulus is a measure of the ability of a material to resist transverse deformations and is a valid index of elastic behaviour for small deformations, after which the material is able to return to its original configuration. Large shearing forces lead to flow and permanent deformation or fracture. The shear modulus is also known as the rigidity. For cubic crystals, the shear modulus G, the anisotropy factor A and the elastic constants are also related by [34]

$$G = \frac{(C_{11} - C_{12})}{2} \tag{10}$$

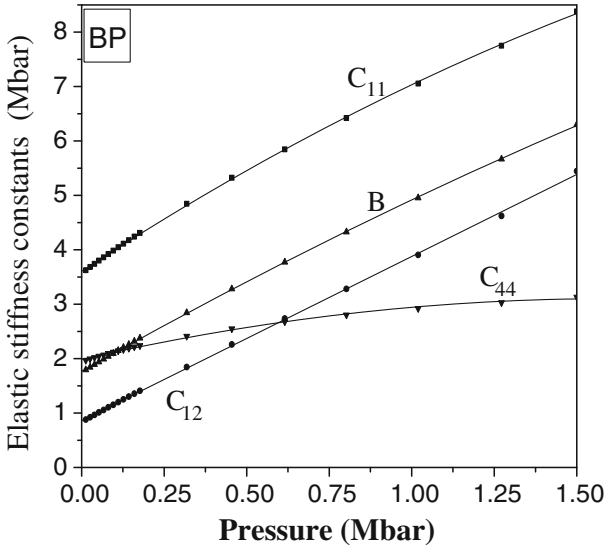

Figure 4. The elastic stiffness constants (shown by curves marked C_{11}, C_{12}, C_{44}) and the bulk modulus (shown by the curve marked B) vs. the hydrostatic pressure of (B3) BP.

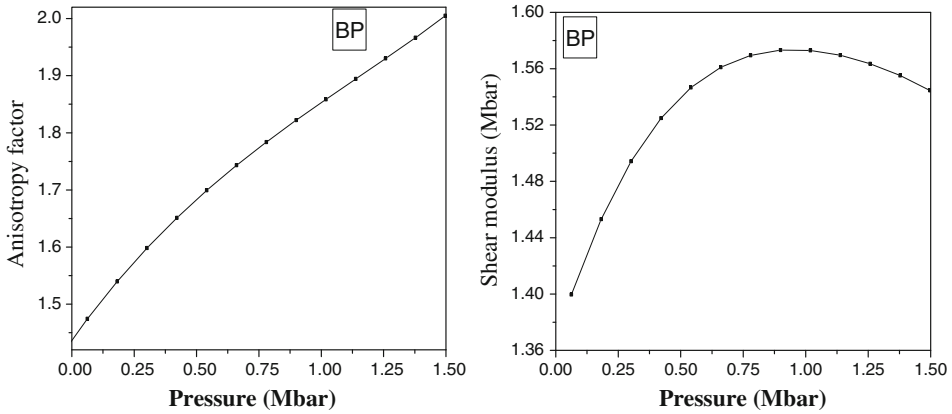

Figure 5. Effect of hydrostatic pressure on the anisotropy factor A and the shear modulus G.

$$A = \frac{2C_{44}}{(C_{11} - C_{12})}. \tag{11}$$

The obtained values of the shear modulus G and the anisotropy factor A of (B3) BP at different pressure are presented in figure 5. As shown in figure 5 we find that the anisotropy factor and the shear modulus G increase gradually with pressure to 1 Mbar, then decrease for pressures greater than this value.

3.2.5 *Stability criteria.* To study the stability of (B3) BP, the calculated values of the elastic constants at normal pressure and under hydrostatic pressure were compared with the generalized stability criteria [36] using the following relations:

$$K = \frac{1}{3}(C_{11} + 2C_{12} + P) > 0, \tag{12a}$$

$$G = \frac{1}{2}(C_{11} - C_{12} - 2P) > 0, \tag{12b}$$

$$G' = C_{44} - P > 0. \tag{12c}$$

The mechanical stability in a cubic crystal requires the following restrictions on the elastic constants: $C_{11} - C_{12} > 0$, $C_{11} > 0$, $C_{44} > 0$, $C_{11} + 2C_{12} > 0$ [37]. The elastic constants at zero pressure obey these stability conditions, including the fact that C_{12} must be smaller than C_{11}. Our calculated elastic constants also obey the cubic stability conditions, $C_{12} < B < C_{11}$.

When pressure is applied to (B3) BP, it transforms from zinc-blende phase into site-ordered NaCl phase [8]. As shown in figure 6 we find that G' decreases gradually with pressure and vanishes at about 1.56 Mbar, and G also decreases to zero but at a higher pressure. Therefore, the phase transition occurs at a much higher pressure of 1.56 Mbar. This value is in good agreement with the theoretical result (1.6 Mbar) of ref. [8], and the deviation is only 1.8%.

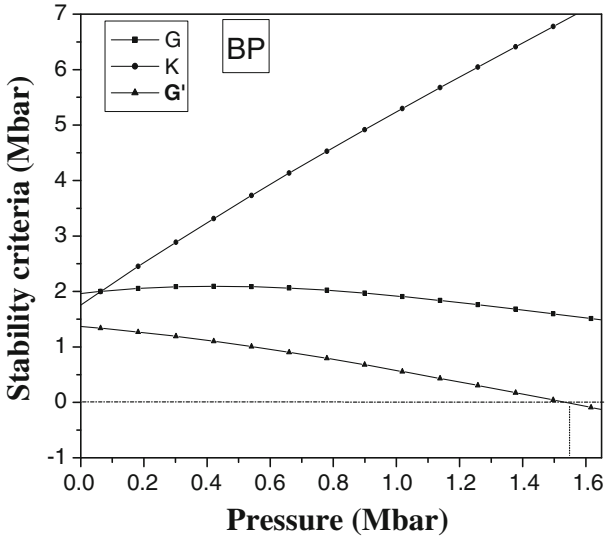

Figure 6. Generalized stability criteria, G, G' and K of (B3) BP.

3.2.6 *Bandgap pressure dependence.* The pressure derivatives of conduction band states [38] and their relative positions are given reasonably well within the LDA. Bouhafs *et al* [39] noted that the LDA tends to underestimate the bandgap pressure coefficients, but it reproduces the experimental trend quite well. The underestimation of the pressure coefficients can probably be attributed to the LDA, but at a small percentage compared to the

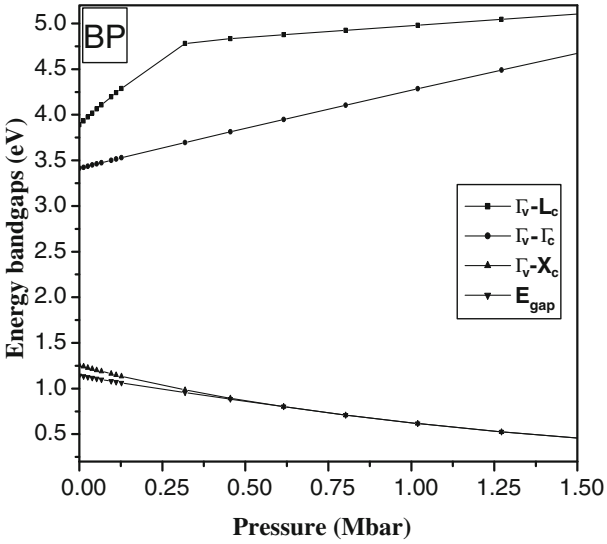

Figure 7. Pressure dependence of the energy bandgaps $E_{\Gamma-\Gamma}$, $E_{\Gamma-X}$, $E_{\Gamma-L}$ and optical energy bandgap E_g.

Table 2. Linear and quadratic pressure coefficients of (B3) BP in comparison with theoretical values [39,40].

	$\Gamma_v-\Gamma_c$		Γ_v-X_c		$\Gamma_v-\Delta_{\min}$		Γ_v-L_c	
	c_1	c_2	c_1	c_2	c_1	c_2	c_1	c_2
Present work	0.95	−0.18	−1.02	0.60	−0.69	0.42	3.83	−3.92
Ref. [39]	1.01	−0.17	−1.03	0.53	−0.72	0.37	3.98	−4.66
Ref. [40]	0.76	−0.019	−1.10	0.41	−0.82	0.23	3.07	−1.96

absolute bandgaps. However, since the *GW*-calculation (see for example, M S Hybertsen and S G Louie, *Phys. Rev. Lett.* **55**, 1418 (1985)) of the self-energy correction to the gap indicates that the correction is typically a rigid shift of the whole conduction band, the pressure coefficient of the bandgap within the LDA is, at least, more reliable than the absolute gap size. They therefore assume that the band states calculated within the LDA show qualitatively correct ordering and dependence on cell volume.

To investigate the effects of hydrostatic pressure on the size of the energy gap and position of the conduction band minimum of the BP compound, the band energies at selected symmetry points are examined as a function of hydrostatic pressure. The results of our calculation for the direct and indirect bandgaps along the high symmetry directions in the Brillouin zone for BP vs. the hydrostatic pressure are shown in figure 7.

At the equilibrium volume, the minimum of the conduction band is found to be at $\Delta_{\min}$ (near X point), rendering this compound an indirect semiconductor with a small ($\Gamma_{15v}-\Delta_{\min}$) optical transition of 1.208 eV. This value is in good agreement with the previous calculations, but it deviates from the result (1.2 eV) of ref. [7] within 0.67%.

As for typical semiconductors, the fundamental gap decreases when the pressure increases (volume is compressed). The bandgap variation under high hydrostatic pressure is very similar to that found in III–V materials [39].

For most semiconductors, the variation of different bandgaps under pressure can be described by the following quadratic expression [40,41]:

$$E_i(P) = E_i(0) + c_1 P + c_2 P^2, \tag{13}$$

where c_1 and c_2 are respectively the linear and quadratic pressure coefficients and they are respectively given by

$$c_1 = \frac{\partial E_i}{\partial p} \text{ in eV Mbar}^{-1}, \qquad c_2 = \frac{\partial^2 E_i}{\partial p^2} \text{ in eV Mbar}^{-2}.$$

The results for the linear and quadratic pressure coefficients are reported in table 2 and compared with the available theoretical data [39,40].

4. Conclusions

Employing PP-PW approach based on density functional theory, within the local density approximation, we studied the effect of hydrostatic pressure on the structural and elastic properties, and the phase transition pressure for boron phosphide in its zinc-blende phase.

A summary of the obtained results is given here as follows:

(1) The calculated equilibrium lattice constant, the bulk modulus and its pressure derivatives are in excellent agreement with the experimental data and the previous calculations reported in the literature.
(2) The calculated unit cell volumes under a series of applied hydrostatic pressure are used to construct the P–V dataset, which was subsequently fitted by the Murnaghan equation.
(3) The pressure phase transition from the zinc-blende phase (B3) to rock-salt phase (B1) of this compound is obtained, it is at around 1.56 Mbar, which is in good agreement with the available theoretical data reported in the literature.
(4) The energy bandgap of this compound at the equilibrium volume is obtained, the minimum of the conduction band is found to be near X point, rendering this compound an indirect semiconductor with a small ($\Gamma_{15v} - \Delta_{min}$) optical transition of 1.208 eV, and this value is also in good agreement with the previous calculations.
(5) The effects of hydrostatic pressure on the size of the energy gap and position of the conduction band minimum of BP are investigated. The linear and quadratic pressure coefficients are also determined, and the results obtained are generally in good agreement with the available theoretical data reported in the literature.

References

[1] J K Furdyana, *J. Appl. Phys.* **64**, R29 (1988)
[2] N Samarth and J K Furdyana, *Proc. IEEE* **78**, 990 (1990)
[3] P Kocinski and M Zbroszczyk, *Semicond. Sci. Technol.* **10**, 1452 (1995)
[4] M J Herrera-Cabrera, P Rodriguez-Hernandez and A Munoz, *Phys. Status Solidi* **223**, 411 (2009)
[5] O A Golikova, *Phys. Status Solidi* **51**, 11 (1979)
[6] Y Kumashiro, *J. Mater. Res.* **5**, 2933 (1990)
[7] R M Wentzcovitch, K J Chang and M L Cohen, *Phys. Rev.* **B34**, 1071 (1986)
[8] R M Wentzcovitch, M L Cohen and P K Lam, *Phys. Rev.* **B36**, 6058 (1987)
[9] R Orlando, R Doveshi, C Roetti and V R Saunders, *J. Phys. Condens. Matter* **2**, 7769 (1990)
[10] Landolt-Bornstein, *New Series: Numerical data & functional relationship in science & technology* (Springer, Berlin, 1982–89) Vols 17a and 22
[11] J A Sanjurjo, E Lopez-Cruz, P Vogi and M Cardona, *Phys. Rev.* **B28**, 4579 (1983)
[12] D Olego and M Cardona, *Phys. Rev.* **B25**, 1151 (1982)
[13] D Olego, M Cardona and P Vogel, *Phys. Rev.* **B25**, 3878 (1982)
[14] S Shinde, A Pandya and P KJha, *Ind. J. Pure Appl. Phys.* **48**, 543 (2010)
[15] E Engel and R M Dreizler, *Density functional theory* (Springer-Verlag, Berlin, Heidelberg, 2011)
[16] The ABINIT computer code, Available online at http://www.abinit.org
[17] J P Perdew, K Burke and M Ernzerhof, *Phys. Rev. Lett.* **77**, 3865 (1996)
[18] N Troullier and J L Martins, *Phys. Rev.* **B43**, 1993 (1991)
[19] H J Monkhorst and J D Pack, *Phys. Rev.* **B13**, 5189 (1976)
[20] F Murnaghan, *Proc. Natl. Acad. Sci. USA* **30**, 244 (1944)
[21] C G Broyden, *J. Inst. Math. Appl.* **6**, 222 (1970)
[22] O A Golikova, *Phys. Status Solidi* **51**, 11 (1979)
[23] G A Slack and S F Bartram, *J. Appl. Phys.* **46**, 89 (1975)

[24] W Wettling and J Windscheih, *Solid State Commun.* **50**, 33 (1984)
[25] W R L Lambrecht and B Segall, *Phys. Rev.* **B43**, 7070 (1991)
[26] Hui Xia, Qing Xia and A L Ruoff, *J. Appl. Phys.* **74**, 1660 (1993)
[27] M L Cohen, *Phys. Rev.* **B32**, 7988 (1985)
[28] L M Liu, S Q Wang and H Q Ye, *J. Phys. Condens. Matter* **17**, 5335 (2005)
[29] J Haglund, G Grimvall, T Jarlborg and A F Guillermet, *Phys. Rev.* **B43**, 14400 (1991)
[30] R C Mota, S C Costa, P S Pizani and J P Rino, *Phys. Rev.* **B71**, 224114 (2005)
[31] H Schlosser, *J. Phys. Chem. Solids* **53**, 855 (1992)
[32] A S Verma, B K Sarkar and V K Jindal, *Pramana – J. Phys.* **74(5)**, 851 (2010)
[33] A S Verma, *Phys. Lett.* **A372**, 7196 (2008)
[34] C Kittel, *Introduction to solid state physics* (John Wiley and Sons, New York, 1953)
[35] O H Nielsen and R M Martin, *Phys. Rev.* **B32**, 3792 (1985)
[36] J Wang and S Yip, *Phys. Rev. Lett.* **71**, 4182 (1993)
[37] M Born and K Huang, *Dynamical theory of crystal lattices* (Clarendon, Oxford, 1954)
[38] S Fahy, K J Chang, S G Louie and M L Cohen, *Phys. Rev.* **B35**, 5856 (1987)
[39] B Bouhafs, H Aourag and M Cartier, *J. Phys. Matter* **12**, 5655 (2000)
[40] S Labidi, H Meradji, S Ghemid, S Meçabih and B Abbar, *J. Optoelectron. Adv. Mater.* **11(7)**, 994 (2009)
[41] M Haase and A P Alivisatos, *J. Phys. Chem.* **96**, 6756 (1992)